Nonlinear Analysis: Modelling and Control, Vilnius, IMI, 2000, No 5

The Influence of the Diffusion Space Geometry on Behavior of some Processes in Biochemistry and Electrochemistry

R. Baronas
Vilnius University, Naugarduko 24, 2600 Vilnius, Lithuania
romas.baronas@maf.vu.lt

F. Ivanauskas
Institute of Mathematics and Informatics,
Akademijos 24, 2600 Vilnius, Lithuania
Vilnius University, Naugarduko 24, 2600 Vilnius, Lithuania
feliksas.ivanauskas@maf.vu.lt

J. Kulys
Institute of Biochemistry, Mokslininku 12, 2600 Vilnius, Lithuania
jkulys@ktl.mii.lt

M. Sapagovas
Institute of Mathematics and Informatics,
Akademijos 24, 2600 Vilnius, Lithuania
sapagovas@ktl.mii.lt

A. Survila
Institute of Chemistry, Goštauto 9, 2600 Vilnius, Lithuania
asurvila@ktl.mii.lt

Received: 18.08.2000
Accepted: 27.09.2000

Abstract

The reaction-diffusion and diffusion equations were applied for modelling of some processes in biochemistry and electrochemistry. Modelling of the amperometric biosensors based on carbon paste electrodes encrusted with a single nonhomogeneous microreactor is analyzed. The mathematical model of the biosensor operation is based on nonstationary reaction-diffusion equations containing a non-linear term given by Michaelis-Menten function. Modelling of a simple redox-electrode reaction, involving two soluble species, is also considered. The model of the

electrode behavior, taking into account the resist layer of the partially blocked electrodes, was expressed as a system of differential equations of the diffusion type with initial and boundary conditions. The mathematical model generalizing both processes: biochemical and electrochemical is presented in this paper. The generalized problem was solved numerically. The finite-difference technique was used for discretisation of the model. Using the numerical solution of the generalized problem, the influence of the size, shape and position of a microreactor as well as the thickness of the resist layer on the current dynamics was investigated.

Keywords: modelling, diffusion, biosensors, partially-blocked electrodes, microreactor.

1. Introduction

More than 200 million people worldwide, approximately half undiagnosed, are estimated to suffer from diabetes [1, 2]. Between 0.6 and 0.7 million new cases are diagnosed each year in the USA. About 0.8 million people are insulin-depend in the USA. People with diabetes measure their blood glucose levels by sticking a finger with a needle to obtain a blood drop that is placed on a test strip and analyzed by a portable instrument. Repeating this procedure several times a day becomes painful, leading many patients, especially the elderly, to perform the procedure infrequently. Furthermore, the accuracy of some blood glucose analyzers is poor. Glucose biosensors appears to be promissing as blood glucose analyzers [3].

Recently, the amperometric biosensors based on carbon paste electrodes (CPEs) encrusted with a single microreactor (MR) have been constructed for the determination of glucose [4, 5]. The MRs were prepared from CPC-silica carrier and were loaded with glucose oxidase (GO), mediator and acceptor.

Starting from the publication by Clark and Lyons [6], biosensors became one of the perspective lines of investigation in analytical devices. In most cases the membrane biosensors were used in the investigation. Mathematical models of behavior of a membrane biosensor are rather widely known [7]. In case of a membrane biosensor, the enzyme electrode has a layer of enzyme immobilised onto the surface of the probe.

In [5] author explored an idea to separate the enzyme and the electron transfer components in a microreactor, the silica particle, and use the well-established carbon paste electrode.

One of the goals of this research is to propose a model allowing us an effective digital simulation of biosensor operation as well as to investigate

the influence of the geometry of a microreactor on the operation of the biosensor.

The mathematical model of the operation of biosensors is based on non-stationary diffusion equations containing a non-linear term related to the enzymatic reaction. In the simplest case, this term is given by Michaelis-Menten equation [8, 9]:

$$\frac{dv}{dt} = -\frac{du}{dt} = \frac{au}{b+u}, \tag{1.1}$$

where a represents the maximal enzymatic rate, b the Michaelis constant, u the substrate concentration, and v the reaction product concentration. Due to the technology of the construction of MR, the number and geometrical shape of the cells, which are filled with glucose oxidase, cannot be precisely defined. The problems in the modelling arise because of possibility to solve analytically such type of equations. In the digital modelling, the nonhomogeneous nature and size of MR, the complexity of the boundary conditions and the overload of calculation are the main problems. Therefore, the model was reduced by the homogenization process [10].

Modelling of a simple redox-electrode reaction, involving two soluble species, is also considered in this paper. Microelectrodes and their ensembles (arrays) have been investigated recently from both theoretical and experimental point of view. A comprehensive review of papers is given in [11].

High diffusion current densities conditioned by radial flows, and low values of ohmic potential drop are most prominent in the case of ultramicroelectrodes, whose characteristic length is less than 20μm [11, 12]. Modern technologies make it possible to manufacture electrodes of very small dimensions (down to $0.2 - 1\mu$m of order) [13], by using different materials.

Because of the currents observed at single electrodes are not high (due to a small area of their surface), the microelectrode ensembles with the above properties are advised to be used for various purposes. The range of application of such microelectrodes is very wide, covering viz. electroanalysis and investigations of kinetics of electrochemical reactions [14, 15, 16], usage in vivo of microsensors modified by enzymes [17], application of microprobes sensitive to various ions in scanning electrochemical microscopy [18], monitoring of zone distribution in electrophoresis, improvement of liquid chromatographic detectors [19], etc.

A hexagonal distribution of unit cells containing active/passive disc electrodes has been analyzed in terms of semi-infinite diffusion in [16, 20, 21]. To simplify quantitative description, the cell was divided into two coaxial spaces, with different regularities of mass transport. Such approach made possible to apply the Laplace transform and to obtain analytical expressions. Usually these expressions involved a parameter γ [20], which used to have a physical sense, but was in fact, a fitting parameter. Experimental data obtained with linear potential sweep (LPS) technique followed the theoretical regularities of the model [21]. Though the employed model electrodes had the photoresist layer of the thickness of $1 - 2\mu$m, in mathematical model the electrode surface was assumed to be flat.

This approach was improved in [22, 23, 24] where the diffusion in limited space (a concept of a pseudo Nerst diffusion layer) was taken into account. In addition, the division of diffusion space into two parts was made by means of a plane parallel to the electrode surface.

Semi-infinite diffusion image is generally used in theoretical works. According to this, the diffusion front may infinitely shift from the electrode surface to the bulk of solution. However, if the measurement time is not very short, it is indispensable to take into consideration the consequences of natural convection as well (see, e.g., [25]).

The electrochemical process includes exchange of current and diffusion. A model allowing us to simulate effectively the electrochemical behavior of partially blocked electrodes under linear potential sweep conditions is proposed in this paper. The model of the electrode behavior was expressed as a system of partial differential equations of the diffusion type with initial and boundary conditions. The proposed model involves the Nerst diffusion layer as well as a resist layer of the inactive site of the electrode surface. The diffusion space adjustment to the electrode surface is divided into equal hexagonal prisms with regular hexagonal bases. For simplicity, a circle whose area is equal to that hexagon is considered.

In the proposed model, the mass transport is regular in the entire diffusion space. The influence of the thickness of the resist layer is investigated is this paper. Specifically it is shown that the influence of 1μm thickness of the resist layer can be significant for relatively small active areas of the partially blocked electrodes.

The mathematical model of the generalized process involving a reaction (enzymatic process) in a microreactor, the charge transfer in active region of an electrode, and the diffusion is presented in this paper. The generalized

problem was solved numerically. The finite-difference technique was used for discretisation of the model. Since the size of MR as well as the size of the resist layer is much less than the size of the diffusion space, the overload of calculation is the main problem in the numerical modelling.

The influence of the size, shape and position of a microreactor as well as the thickness of the resist layer on the current dynamics was investigated. The dependence of the maximal current on the geometry of the diffusion space was considered.

2. Mathematical Modelling

Let us describe a model of behavior of a biosensor based on the nonhomogeneous microreactor as well as a model of electrochemical behavior of partially blocked electrodes under linear potential sweep.

2.1. A Model of Behavior of a Biosensor based on the nonhomogeneous Microreactor

Let $\overline{\Omega}$ be the finite closed area of the container (buffer solution) which was filled with some substrate, and Ω_0 the area of MR ($\Omega_0 \subset \Omega$). Let Γ be the whole surface of the container ($\overline{\Omega} = \Omega \cup \Gamma$), and Γ_1 ($\Gamma_1 \subset \Gamma$) only the base of the container. Γ_1 also denotes the surface of the electrode.

Since the microreactor was constructed from CPC-silica carrier (CPC) and was loaded with glucose oxidase (GO), let the whole MR area Ω_0 consist of two areas: Ω_{0C}, the CPC-carrier, and Ω_{0G}, the glucose oxidase ($\Omega_0 = \Omega_{0C} \cup \Omega_{0G}$) (figure 2.1).

The operation of the biosensor includes heterogeneous enzymatic process (reaction) and diffusion. The stimulus of the reaction is MR, but the reaction performs only in the area Ω_{0G} of MR which was filled with glucose oxidase. The mathematical model [26] consists of a system of the following non-linear differential equations of reaction-diffusion type:

$$\frac{\partial u}{\partial t} = \text{div } (D \text{ grad } u) - f(u), \tag{2.1}$$

$$\frac{\partial v}{\partial t} = \text{div } (D \text{ grad } v) + f(u), \tag{2.2}$$

$$D|_{\Omega_{0G}} = D|_{\Omega \setminus \Omega_0} = d, \quad D|_{\Omega_{0C}} = 0, \tag{2.3}$$

$$f|_{\Omega_{0G}} = au/(b+u), \quad f|_{\Omega_{0C}} = f|_{\Omega \setminus \Omega_0} = 0, \tag{2.4}$$

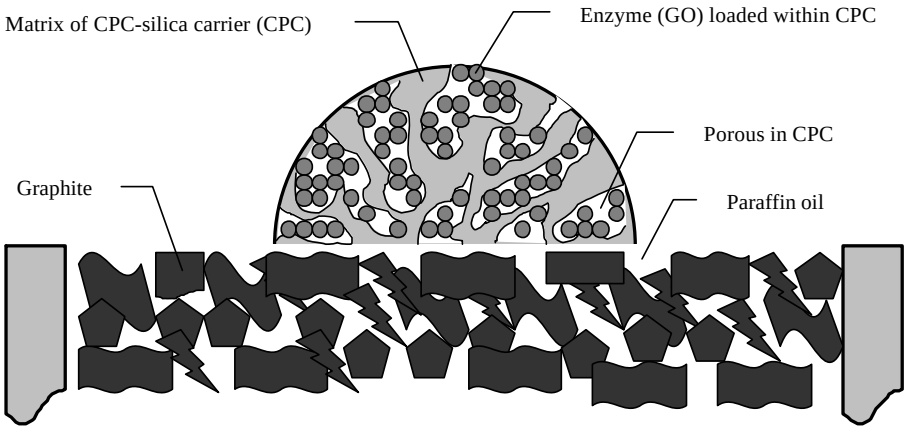

Fig. 2.1: A principal structure of a nonhomogeneous microreactor was constructed from CPC-silica carrier and was loaded with glucose oxidase. The average size of a cell which is filled with glucose oxidase is much less than the size of MR. The geometrical shapes of cells are not precisely defined.

where u is the substrate concentration, v is the concentration of the reaction product, d is the constant diffusion rate of the substrate and reaction product, a is the maximal enzymatic rate, b is the Michaelis constant, and t is time. The initial conditions ($t = 0$) are

$$u|_{\Omega_0} = 0, \quad u|_{\overline{\Omega}\setminus\Omega_0} = u_0, \quad v|_{\overline{\Omega}} = 0. \tag{2.5}$$

When an electrode is polarised, the concentration of the reaction product at the electrode surface is being reduced to zero. This is used in the boundary conditions ($t > 0$) given by

$$\frac{\partial u}{\partial \mathrm{n}}\Big|_{\Gamma} = 0, \quad \frac{\partial v}{\partial \mathrm{n}}\Big|_{\Gamma\setminus\Gamma_1} = 0, \quad v|_{\Gamma_1} = 0, \tag{2.6}$$

where $\partial u/\partial \mathrm{n}|_{\Gamma}$ is a derivative of u with respect to the internal normal direction to the surface Γ.

Due to the technology of the construction of MR, the number of cells which are filled with glucose oxidase is very large, so an average size of

a cell is much less than the size of MR. The number of the cells and the geometrical shape of the cells cannot be precisely defined. For that reason, it is hopeless to solve (2.1)-(2.6) analytically and even to design an effective algorithm for the numerical calculations.

It was assumed that MR is a periodic medium, and the model (2.1)-(2.6) was reduced by the homogenization process [10]. Let c be the ratio of the volume of the glucose oxidase which fills the MR cells to the volume of entire MR (it is easy to calculate this ratio experimentally), i.e., $c = volume(\Omega_{0G})/volume(\Omega_0)$. By using the homogenization process, the definition of the non-linear term related to the enzymatic reaction was simplified and the model was reduced to

$$\frac{\partial \overline{u}}{\partial t} = \text{div } (\overline{D} \text{ grad } \overline{u}) - cf(\overline{u}), \tag{2.7}$$

$$\frac{\partial \overline{v}}{\partial t} = \text{div } (\overline{D} \text{ grad } \overline{v}) + cf(\overline{u}), \tag{2.8}$$

$$\overline{D}|_{\Omega \setminus \Omega_0} = d, \quad \overline{D}|_{\Omega_0} = \overline{d}, \tag{2.9}$$

$$f|_{\Omega_0} = a\overline{u}/(b+\overline{u}), \quad f|_{\Omega \setminus \Omega_0} = 0, \tag{2.10}$$

where $\overline{u} \approx u$, $\overline{v} \approx v$, and $\overline{d}$ is the average diffusion rate in the entire area of MR (Ω_0).

The initial conditions and the boundary conditions are the same as above ((2.5) and (2.6), respectively).

The value $\overline{d}$ of the diffusion rate in the area of MR (Ω_0) depends on the diffusion rate d, the geometry of MR, and the ratio c [10]. If d_{go} is a diffusion rate in enzyme (GO), and d_{cpc} is a diffusion rate in silica carrier, then the average diffusion rate $\overline{d}$ in the entire media can be chosen employing the following condition:

$$\frac{2d_{go}d_{cpc}}{d_{go}+d_{cpc}} \leq \overline{d} \leq \frac{d_{go}+d_{cpc}}{2}. \tag{2.11}$$

Because of (2.11) and assumption that $d_{go} = d, d_{cpc} = 0$, the average diffusion rate $\overline{d}$ must satisfy the condition

$$0 \leq \overline{d} \leq d/2. \tag{2.12}$$

The biosensor current density i at time t is proportional to the concentration gradient of the product of reaction near the surface of the electrode:

$$i(t)\big|_{\Gamma_1} = nF\overline{D}\frac{\partial v}{\partial \mathrm{n}}, \tag{2.13}$$

where n is a number of electrons, and F is Faraday constant.

The total biosensor current $I(t)$ at time t can be expressed by integrating of (2.13) over the entire surface of the electrode (the base of the buffer solution):

$$I(t) = \iint_{\Gamma_1} i(t) d\Gamma_1. \tag{2.14}$$

The container was modelled as a right cylinder with circles of radius R in bases and altitude of H. MR was modelled as a rotation figure. Particularly, MR was modelled as a hemisphere of radius R_0. MR was placed on the center of the base of the container (figure 2.1).

Due to symmetry, the model (2.7)-(2.10),(2.5),(2.6) may be written in two cylindrical coordinates (r, z) with

$$\begin{aligned}
\Omega =& \{(r,z) : 0 < r < R, 0 < z < H\},\\
\Omega_0 =& \{(r,z) : r^2 + z^2 < R_0^2, z > 0\},\\
\Gamma_1 =& \{(r,0) : 0 \le r \le R\},\\
\Gamma =& \{(0,z) : 0 < z \le H\} \cup\\
& \{(R,z) : 0 < z \le H\} \cup\\
& \{(r,H) : 0 < r < R\} \cup \Gamma_1.
\end{aligned} \tag{2.15}$$

The definition of Ω_0 in (2.15) depends on a shape of MR. Several other geometrical shapes of MR differing from the hemisphere were used in the investigation of the biosensor behavior.

2.2. A Model of electrochemical Behavior of partially blocked Electrodes

Consider a simple redox-electrode reaction:

$$O + ne \rightleftharpoons R, \tag{2.16}$$

involving only soluble species. The redox process includes a charge transfer and diffusion. It was assumed that mass transport obeys a finite diffusion regime within a Nerst layer from the electrode/electrolyte boundary. Because of the thickness of the Nerst layer may be different for species O and

R, let us define two finite closed areas: $\overline{\Omega}_O = \Omega_O \cup \Gamma_O$ and $\overline{\Omega}_R = \Omega_R \cup \Gamma_R$ with the boundary Γ_O and Γ_R, respectively. Let us notice that either $\Omega_O \subseteq \Omega_R$ or $\Omega_R \subseteq \Omega_O$. Let Γ_R^N (Γ_O^N, respectively) be the upper surface (Nerst layer boundary) of the space $\overline{\Omega}_R$ ($\overline{\Omega}_O$, respectively) ($\Gamma_R^N \subset \Gamma_R$, $\Gamma_O^N \subset \Gamma_O$).

The surface of a solid electrode is generally composed of active (uncovered) and inactive (covered) sites. Since, the charge transfer occurs in the active region of the electrode only, let Γ_{act} be the active region of the electrode ($\Gamma_{act} \subset \Gamma_R$, $\Gamma_{act} \subset \Gamma_O$).

The mathematical model of the reaction (2.16) can be written as a system of partial differential equations of the diffusion type:

$$\frac{\partial C_R}{\partial t} = D_R \Delta C_R, \tag{2.17}$$

$$\frac{\partial C_O}{\partial t} = D_O \Delta C_O, \tag{2.18}$$

where Δ is the Laplace operator, C_R and C_O are the concentrations of the species R and O, respectively, D_R, D_O are the diffusion coefficients, and t is the time elapsed since the beginning of the electrolysis.

The initial conditions ($t = 0$) are

$$C_R|_{\overline{\Omega}_R} = C_R^0, \quad C_O|_{\overline{\Omega}_R} = C_O^0, \tag{2.19}$$

where C_R^0 and C_O^0 are the initial concentration of the species in the container.

The boundary conditions ($t > 0$) are

$$C_R|_{\Gamma_R^N} = C_R^0, \quad C_O|_{\Gamma_O^N} = C_O^0, \tag{2.20}$$

$$\frac{\partial C_R}{\partial \mathrm{n}}\Big|_{\Gamma \setminus (\Gamma_{act} \cup \Gamma_R^N)} = \frac{\partial C_O}{\partial \mathrm{n}}\Big|_{\Gamma \setminus (\Gamma_{act} \cup \Gamma_O^N)} = 0, \tag{2.21}$$

$$nFD_R \frac{\partial C_R}{\partial \mathrm{n}}\Big|_{\Gamma_{act}} = -nFD_O \frac{\partial C_O}{\partial \mathrm{n}}\Big|_{\Gamma_{act}} = i(t) \tag{2.22}$$

with

$$\begin{aligned} i(t)\Big|_{\Gamma_{act}} = i_0 \Bigg(& \frac{C_R}{C_R^0} \exp\left(-\frac{\alpha n F}{RT}\left(E_{eq} - E(t)\right)\right) - \\ & - \frac{C_O}{C_O^0} \exp\left(\frac{(1-\alpha) n F}{RT}\left(E_{eq} - E(t)\right)\right) \Bigg), \end{aligned} \tag{2.23}$$

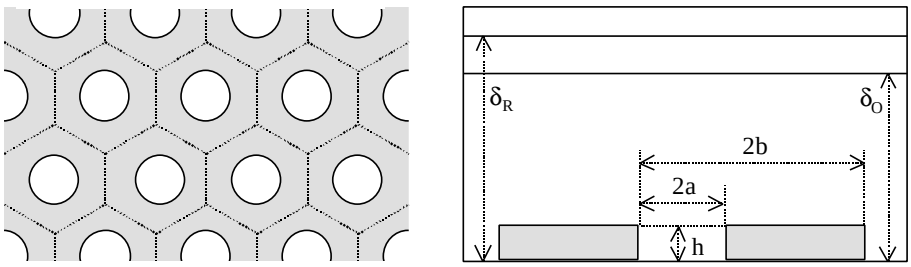

Fig. 2.2: A principal structure of (a) partially blocked electrode and (b) the profile at z plane. Shaded areas indicate the resist layer. The figure is not to scale.

where i is the current density, $E(t)$ is the electrode potential, E_{eq} is the equilibrium potential of the reaction (2.16), α is the anodic transfer coefficient, i_0 is the standard rate constant, $\partial/\partial \mathrm{n}|_\Gamma$ denotes a derivative with respect to the internal normal direction to the surface Γ, F is the Faraday constant, R is the gas constant, and T is the absolute temperature.

The total current $I(t)$ can be expressed by integrating (2.23) over the whole surface of the active region of the electrode:

$$I(t) = \iint_{\Gamma_{act}} i(t) d\Gamma_{act}, \tag{2.24}$$

For a single cyclic potential sweep, the electrode potential-time function can be written as

$$E(t) = \begin{cases} E_{eq} - vt, & 0 \le t \le t_r, \\ E_{eq} - 2vt_r + vt, & t > t_r, \end{cases} \tag{2.25}$$

where v is the sweep rate and t_r is the time of reversal of the linear potential-time sweep [21].

The mathematical model (2.17)-(2.23) was applied for digital simulation of real experiments. The principal structure of the surface of partially blocked electrodes, used in the experiments, is shown in figure 2.2a, where m circular active regions of radius a are arranged in a rigid hexagonal array. Due to the symmetric distribution of the active sites, leaving out of account

the resist layer, the diffusion space adjustment to the electrode surface may be divided into m equal hexagonal prisms with regular hexagonal bases. For simplicity, it is reasonable to consider a circle of radius b (figure 2.2b) whose area is equal to that of the hexagon and to regard one of the cylinders as a unit cell of the diffusion space [21]. Due to the symmetry of a cylinder, we may consider only a quarter of the cylinder. Now, taking into account the resist layer of thickness h (figure 2.2b), the mathematical model (2.17)-(2.23) of the reaction (2.16) for partially blocked electrodes, shown in figure 2.2, may be written in cylindrical coordinates (r, z) with

$$\begin{aligned}
\Gamma_{act} =& \{(r,z) : 0 \le r \le a, z = 0\}, \\
\Gamma_O^N =& \{(r,z) : 0 \le r \le b, z = \delta_O\}, \\
\Gamma_R^N =& \{(r,z) : 0 \le r \le b, z = \delta_R\}, \\
\overline{\Omega}_O =& \{(r,z) : 0 \le r \le a, 0 \le z \le \delta_O\} \cup \\
& \{(r,z) : a \le r \le b, h \le z \le \delta_O\}, \\
\overline{\Omega}_R =& \{(r,z) : 0 \le r \le a, 0 \le z \le \delta_R\} \cup \\
& \{(r,z) : a \le r \le b, h \le z \le \delta_R\},
\end{aligned} \tag{2.26}$$

where δ_O and δ_R is the thickness of the Nerst layer for species O and R, respectively.

3. Generalized Problem

We generalized the model of a biosensor based on MR and the model of partially blocked electrodes to a model having all the features of both initial models. The reason of such generalization was an idea to develop a parameterized effective algorithm for numerical simulation of both initial processes. The main aim of the generalization was to reuse existing program code more efficiently, and increase the productivity of realization of similar models. For that reason some parameters were introduced to the generalized model without necessity in point of view of the models defined above. On the other hand, generalization allows us to model some additional features of the processes discussed above, e.g., to simulate electrochemical behavior of partially blocked electrodes with nonhomogeneous active areas (the active area consists of the more active area and the less active one).

The generalized model can be used to simulate behavior of the electrochemical process when immobilized enzyme is fastened upon the flat surface of an indicator electrode. A model of a flat biosensor where electrochemical reaction (2.16) coupled with an enzyme reaction, characterized by

Michaelis-Menten equation (1.1) can be found in [27]. So, the generalized model can be treated as a model of a really possible process.

3.1. Definition of the Generalized Problem

Let $\overline{G}_\alpha = G_\alpha \cup \Gamma_\alpha$ $(\alpha = 1, 2)$ be a finite closed area with the boundary Γ_α, and G_0 an area (may be empty) inside the area G_α, i.e., $G_0 \subset G_\alpha$, $\alpha = 1, 2$. Let Γ_{act} be a subset of the boundary Γ_α lying at the plane $z = 0$, i.e., $\Gamma_{act} \subset \Gamma_\alpha|_{z=0}$, $\alpha = 1, 2$.

The generalized problem was defined as a boundary-value problem with initial conditions. Consider a system of the following non-linear differential equations of the reaction-diffusion type expressed in two cylindrical space coordinates (r, z):

$$\frac{\partial u}{\partial t} = L_1^{d_1} u + L_2^{d_1} u - cf(u), \quad (r, z) \in G_1, \tag{3.1}$$

$$\frac{\partial v}{\partial t} = L_1^{d_2} v + L_2^{d_2} v + cf(u), \quad (r, z) \in G_2, \tag{3.2}$$

where operator $L_\beta^d u$ $(\beta = 1, 2)$ is defined as

$$L_1^d u = \frac{1}{r}\frac{\partial}{\partial r}\left(rd(r, z)\frac{\partial u}{\partial r}\right), \tag{3.3}$$

$$L_2^d u = \frac{\partial}{\partial z}\left(d(r, z)\frac{\partial u}{\partial z}\right), \tag{3.4}$$

c is a constant, and the function $f(u)$ is defined as

$$f(u) = \begin{cases} \dfrac{au}{b+u}, & (r, z) \in G_0, \\ 0, & (r, z) \in (G_1 \cup G_2) \setminus G_0. \end{cases} \tag{3.5}$$

The initial conditions $(t = 0)$ are

$$u(r, z, 0) = u_0(r, z), \quad (r, z) \in \overline{G}_1, \tag{3.6}$$

$$v(r, z, 0) = v_0(r, z), \quad (r, z) \in \overline{G}_2. \tag{3.7}$$

The boundary conditions $(t \in (0, T])$ are

$$\varphi_{11}(r,t)\frac{\partial u}{\partial z}+\varphi_{12}(r,t)u+\varphi_{13}(r,t)v=0, \quad (r,z)\in\Gamma_{act}, \tag{3.8}$$

$$\varphi_{21}(r,t)\frac{\partial v}{\partial z}+\varphi_{22}(r,t)u+\varphi_{23}(r,t)v=0, \quad (r,z)\in\Gamma_{act}, \tag{3.9}$$

$$\psi_{11}(r,z)\frac{\partial u}{\partial \mathrm{n}}+\psi_{12}(r,z)u=\psi_{13}(r,z), \quad (r,z)\in\Gamma_1\backslash\Gamma_{act}, \tag{3.10}$$

$$\psi_{21}(r,z)\frac{\partial v}{\partial \mathrm{n}}+\psi_{22}(r,z)v=\psi_{23}(r,z), \quad (r,z)\in\Gamma_2\backslash\Gamma_{act}, \tag{3.11}$$

where $\partial/\partial\mathrm{n}$ denotes a derivative with respect to the internal normal direction to the surface, and $\varphi_{\alpha\beta}(r,t)$, $\psi_{\alpha\beta}(r,z)$ are functions, $\alpha=1,2$; $\beta=1,2,3$.

Let $I(t)$ be a function defined as

$$I(t)=nF\int_0^{2\pi}\int_{\Gamma_{act}} d_2(r,z)\frac{\partial v}{\partial z}\Big|_{\Gamma_{act}} r\,dr\,d\varphi, \tag{3.12}$$

where F is the Faraday constant, n is a coefficient (the number of electrons).

We solve the system of equations (3.1)-(3.11) with

$$\begin{aligned}\overline{G}_\alpha =&\{(r,z): 0\le r\le A, 0\le z\le \delta_\alpha\}\cup\\ &\{(r,z): A\le r\le R, B\le z\le \delta_\alpha\},\\ \Gamma_{act} =&\{(r,z): 0\le r\le A, z=0\}, \Gamma_{act}\subset\Gamma_\alpha, \alpha=1,2.\end{aligned} \tag{3.13}$$

3.2. Numerical Solution of the Generalized Problem

Closed mathematical solutions are not usually possible when analytically solving the differential equations with complex diffusion space and boundary conditions as well as the variable diffusion coefficient, therefore the problem represented by (3.1)-(3.11) was solved numerically. The finite-difference technique [28] was used for discretisation of the model. This technique allows us to solve effectively the differential equations with rather complex diffusion space and boundary conditions as well as the variable diffusion coefficients. The similar equations of diffusion as (3.1)-(3.11) with various boundary conditions have been investigated in [29, 30].

We introduced non-uniform grids in r and z directions, while an uniform grid was used in the direction t:

$$\begin{aligned}
\widehat{\omega}_h =&\{r_i \in (0,R), r_i = r_{i-1} + h_i, i = 1,2,\ldots,I,\ldots,N-1\},\\
&r_0 = 0, r_N = R, r_I = A;\\
\widehat{\omega}_{\alpha l} =&\{z_j \in (0,\delta_\alpha), z_j = z_{j-1} + l_{\alpha j}, j = 1,2,\ldots,J,\ldots,M_\alpha - 1\},\\
&z_0 = 0, z_{M_\alpha} = \delta_\alpha, z_J = B, \alpha = 1,2;\\
\omega_\tau =&\{t_k = k\tau, k = 1,2,\ldots,K\}, \tau K = T;\\
\widehat{\omega}_\alpha =&((\widehat{\omega}_h \times \widehat{\omega}_{\alpha l}) \setminus \{(r_i,z_j), i \geq I, j \leq J\}) \cup \{(r_I, z_J)\}, \alpha = 1,2.
\end{aligned} \tag{3.14}$$

Let us assume the following:

$$\begin{aligned}
&u_{ij} = u(r_i,z_j,t), \quad v_{ij} = v(r_i,z_j,t), \quad d_{\alpha,ij} = d_\alpha(r_i,z_j),\\
&i = 0,1,\ldots,N, \quad j = 0,1,\ldots,M_\alpha, \quad \alpha = 1,2;
\end{aligned} \tag{3.15}$$

$$\begin{aligned}
&r_{i\pm1/2} = (r_i + r_{i\pm1})/2, \quad h_{i+1/2} = (h_i + h_{i+1})/2,\\
&l_{\alpha,j+1/2} = (l_{\alpha,j} + l_{\alpha,j+1})/2,\\
&d_{\alpha,i\pm1/2,j} = (d_{\alpha,ij} + d_{\alpha,i\pm1,j})/2, \quad d_{\alpha,i,j\pm1/2} = (d_{\alpha,ij} + d_{\alpha,i,j\pm1})/2,\\
&i = 0,1,\ldots,N-1, \quad j = 0,1,\ldots,M_\alpha - 1, \quad \alpha = 1,2.
\end{aligned} \tag{3.16}$$

The terms (3.3),(3.4) were approximated with the following difference operators:

$$\Lambda_1^d u = \frac{1}{r_i h_{i+1/2}} \left(r_{i+1/2} d_{i+1/2,j} \frac{u_{i+1,j} - u_{ij}}{h_{i+1}} - r_{i-1/2} d_{i-1/2,j} \frac{u_{ij} - u_{i-1,j}}{h_i} \right) \tag{3.17}$$

$$\Lambda_2^{d,\alpha} u = \frac{1}{l_{\alpha,j+1/2}} \left(d_{i,j+1/2} \frac{u_{i,j+1} - u_{ij}}{l_{\alpha,j+1}} - d_{i,j-1/2} \frac{u_{ij} - u_{i,j-1}}{l_{\alpha,j}} \right), \alpha = 1,2. \tag{3.18}$$

We relate the system of equations (3.1),(3.2) with the following difference scheme applying the variable direction method:

$$\frac{u^{(k+1/2)} - u^{(k)}}{0.5\tau} = \Lambda_1^{d_1} u^{(k+1/2)} + \Lambda_2^{d_1,1} u^{(k)} - \gamma_{ij} \frac{a u^{(k+1/2)}}{b + u^{(k)}}, (r_i,z_j) \in \widehat{\omega}_1, \tag{3.19}$$

$$\frac{v^{(k+1/2)} - v^{(k)}}{0.5\tau} = \Lambda_1^{d_2} v^{(k+1/2)} + \Lambda_2^{d_2,2} v^{(k)} + \gamma_{ij} \frac{a u^{(k+1/2)}}{b + u^{(k+1/2)}}, (r_i,z_j) \in \widehat{\omega}_2, \tag{3.20}$$

$$\frac{u^{(k+1)} - u^{(k+1/2)}}{0.5\tau} = \Lambda_1^{d_1} u^{(k+1/2)} + \Lambda_2^{d_1,1} u^{(k+1)} - \gamma_{ij} \frac{a u^{(k+1)}}{b + u^{(k+1/2)}}, (r_i,z_j) \in \widehat{\omega}_1, \tag{3.21}$$

$$\frac{v^{(k+1)}-v^{(k+1/2)}}{0.5\tau}=\Lambda_1^{d_2}v^{(k+1/2)}+\Lambda_2^{d_2,2}v^{(k+1)}+\gamma_{ij}\frac{au^{(k+1)}}{b+u^{(k+1/2)}},(r_i,z_j)\in\widehat{\omega}_2, \tag{3.22}$$

where

$$\gamma_{ij}=\begin{cases} c, & (r_i,z_j)\in G_0,\\ 0, & (r_i,z_j)\in (G_1\cup G_2)\setminus G_0. \end{cases} \tag{3.23}$$

The initial conditions (3.6),(3.7) were approximated by

$$u_{i,j}=u^0_{i,j},\quad (r_i,z_j)\in\widehat{\overline{\omega}}_1, \tag{3.24}$$

$$v_{i,j}=v^0_{i,j},\quad (r_i,z_j)\in\widehat{\overline{\omega}}_2. \tag{3.25}$$

Let us assume the following:

$$\begin{aligned} &\varphi_{\alpha\beta,i}=\varphi_{\alpha\beta}(r_i,t),\quad (r_i,0)\in\left(\widehat{\overline{\omega}}_\alpha\cap\Gamma_{act}\right),\\ &\psi_{\alpha\beta,i,j}=\psi_{\alpha\beta}(r_i,z_j,t),\quad (r_i,z_j)\in\left(\widehat{\overline{\omega}}_\alpha\cap(\Gamma\setminus\Gamma_{act})\right),\\ &\alpha=1,2,\quad \beta=1,2,3. \end{aligned} \tag{3.26}$$

The boundary conditions (3.8),(3.9) were approximated by

$$\varphi_{11,i}\frac{u_{i,1}-u_{i,0}}{l_{11}}+\varphi_{12,i}u_{i,0}+\varphi_{13,i}v_{i,0}=0,\quad 0\le i\le I, \tag{3.27}$$

$$\varphi_{21,i}\frac{v_{i,1}-v_{i,0}}{l_{21}}+\varphi_{22,i}u_{i,0}+\varphi_{23,i}v_{i,0}=0,\quad 0\le i\le I, \tag{3.28}$$

The boundary conditions (3.10),(3.11) were approximated by

$$\psi_{11,i,J}\frac{u_{i,J+1}-u_{i,J}}{l_{1J+1}}+\psi_{12,i,J}u_{i,J}=\psi_{13,i,J},\quad I\le i\le N, \tag{3.29}$$

$$\psi_{21,i,J}\frac{v_{i,J+1}-v_{i,J}}{l_{2J+1}}+\psi_{22,i,J}v_{i,J}=\psi_{23,i,J},\quad I\le i\le N, \tag{3.30}$$

$$\psi_{11,i,M_1}\frac{u_{i,M_1-1}-u_{i,M_1}}{l_{1\,M_1}}+\psi_{12,i,M_1}u_{i,M_1}=\psi_{13,i,M_1},\quad 0\le i\le N, \tag{3.31}$$

$$\psi_{21,i,M_1}\frac{v_{i,M_2-1}-v_{i,M_2}}{l_{2M_2}}+\psi_{22,i,M_2}v_{i,M_2}=\psi_{23,i,M_2},\quad 0\le i\le N, \tag{3.32}$$

$$\psi_{11,0,j}\frac{u_{1,j}-u_{0,j}}{h_1}+\psi_{12,0,j}u_{0,j}=\psi_{13,0,j},\quad 0\le j\le M_1, \tag{3.33}$$

$$\psi_{21,0,j}\frac{v_{1,j}-v_{0,j}}{h_1}+\psi_{22,0,j}v_{0,j}=\psi_{23,0,j},\quad 0\le j\le M_2, \tag{3.34}$$

$$\psi_{11,I,j}\frac{u_{I-1,j}-u_{I,j}}{h_I}+\psi_{12,I,j}u_{I,j}=\psi_{13,I,j},\quad 0\le j\le J, \tag{3.35}$$

$$\psi_{21,I,j}\frac{v_{I-1,j}-v_{I,j}}{h_I}+\psi_{22,I,j}v_{I,j}=\psi_{23,I,j},\quad 0\le j\le J, \tag{3.36}$$

$$\psi_{11,N,j}\frac{u_{N-1,j}-u_{N,j}}{h_N}+\psi_{12,N,j}u_{N,j}=\psi_{13,N,j},\quad J\le j\le M_1, \tag{3.37}$$

$$\psi_{21,N,j}\frac{v_{N-1,j}-v_{N,j}}{h_N}+\psi_{22,N,j}v_{N,j}=\psi_{23,N,j},\quad J\le j\le M_2. \tag{3.38}$$

Let us notice, that the implicit of (3.22) can be increased by replacing the term $au^{(k+1)}/(b+u^{(k+1/2)})$ with $au^{(k+1)}/(b+u^{(k+1)})$ if $\varphi_{13}(r,t)=0$, $\forall(r,t)\in([0,A]\times(0,T])$ in (3.8). This increase of implicit may be used in modelling of biosensor based on microreactor.

The difference scheme (3.19) - (3.38) is implicit and linear. The equations (3.24),(3.25) allow us to calculate a solution of the problem on the layer $t=t_0=0$. When a solution on a layer t_k is calculated, a solution on the next layer $t=t_{k+1}$ can be effectively calculated using these steps:

1. Calculate values of $u^{(k+1/2)}$ solving systems of linear equations (3.19), (3.33), (3.35), (3.37) for all $j=M_1-1,\dots,J,\dots,1$. Use a value of $u_{I+1,J}$ calculated from $u_{I+1,J+1}$ using (3.29) in solving the system for $j=J$.

2. Calculate values of $v^{(k+1/2)}$ solving systems of linear equations (3.20), (3.34), (3.36), (3.38) for all $j=M_2-1,\dots,J,\dots,1$ using values of $u^{(k+1/2)}$ which were calculated in step 1. Use a value of $v_{I+1,J}$ calculated from $v_{I+1,J+1}$ using (3.30) in solving the system for $j=J$.

3. Calculate values of $u^{(k+1)}$ and $v^{(k+1)}$ solving systems of linear equations (3.21), (3.27), (3.29), (3.31) and (3.22), (3.28), (3.30), (3.32) for all $i=1,\dots,I,\dots,N$. Use a value of $u_{I,J-1}$ and $v_{I,J-1}$ calculated from $u_{I-1,J-1}$ and $v_{I-1,J-1}$ using (3.35) and (3.36), respectively, in solving the system for $i=I$.

The values of $u^{(k+1)}$ and $v^{(k+1)}$ (step 3) can not be calculated independently from each other (like it was done in step 1 and 2) because of boundary condition (3.27), which relates $u_{i,0}^{(k+1)}$ and $v_{i,0}^{(k+1)}$ for all $i=0,\dots,I$. The step 3 can be splited into two sequential steps: calculation of $u^{(k+1)}$ and calculation of $v^{(k+1)}$ in a special case of $\varphi_{13}(r,t)=0$, $\forall(r,t)\in([0,A]\times(0,T])$ in (3.8).

The systems of linear equations, which are solved in the all three steps above, can be solved effectively because of the tridiagonality of the matrices of the systems.

Function $I(t)$, which was introduced in (3.12), can be approximated as

$$I_k = 0.5nF \sum_{i=0}^{I-1} d_{2_{i+1/2,1/2}} \frac{\left(v_{i+1/2,1} - v_{i+1/2,0}\right)}{l_{21}} \pi \left(r_{i+1}^2 - r_i^2\right) \tag{3.39}$$

for all $k = 1, 2, \ldots, K$ (K was defined in (3.14)).

4. Simulation of the Biosensor Action

4.1. Numerical Simulation of the Behavior of the Biosensor

The numerical solution (3.19) - (3.38) of the generalized problem (3.1)-(3.11) was used for digital simulation of behavior of the amperometric biosensors based on the carbon paste electrodes encrusted with a single nonhomogeneous microreactor.

The mathematical model (2.7)-(2.10), (2.5), (2.6), (2.14) of a biosensor based on the nonhomogeneous MR can be expressed as a special case of the model (3.1) - (3.11) assuming the following:

$$\begin{array}{l}
u = \overline{u}, \quad v = \overline{v}, \\
\delta_1 = \delta_2 = H, \\
A = R, \quad R = R, \quad B = 0, \quad G_1 = G_2 = \Omega, \\
G_0 = \{(r,z) : r^2 + z^2 < R_0^2, z > 0\}, \\
\Gamma_{act} = \{(r,z) : 0 \le r \le R, z = 0\}, \\
u_0(r,z) = \left\{ \begin{array}{ll} 0, & (r,z) \in G_0, \\ u_0, & (r,z) \in (\overline{G_1} \cup \overline{G_2}) \setminus G_0, \end{array} \right. \\
v_0(r,z) = 0, \\
d_1(r,z) = d_2(r,z) = \left\{ \begin{array}{ll} \overline{d}, & (r,z) \in G_0, \\ d, & (r,z) \in (G_1 \cup G_2) \setminus G_0, \end{array} \right. \\
\varphi_{11}(r,t) = 1, \quad \varphi_{12}(r,t) = 0, \quad \varphi_{13}(r,t) = 0, \\
\varphi_{21}(r,t) = 0, \quad \varphi_{22}(r,t) = 0, \quad \varphi_{23}(r,t) = 1, \\
\psi_{11}(r,z) = 1, \quad \psi_{12}(r,z) = 0, \quad \psi_{13}(r,z) = 0, \\
\psi_{21}(r,z) = 1, \quad \psi_{22}(r,z) = 0, \quad \psi_{23}(r,z) = 0.
\end{array} \tag{4.1}$$

Since Γ_1 in (2.15) and Γ_{act} in (4.1) denotes the same area, the total current $I(t)$ can be expressed with (3.12) and calculated by using (3.39).

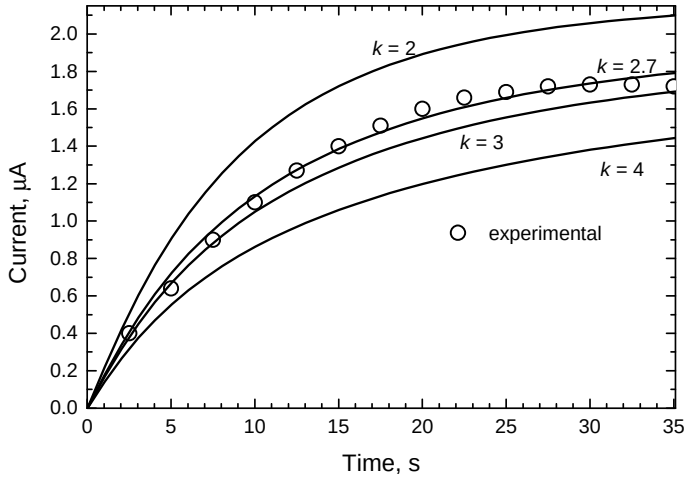

Fig. 4.1: The dynamics of the current of the model biosensor [4, 5]. The microreactor was modelled as hemiellipsoid of revolution. The average diffusion rate $\overline{d}$ in MR was equal to d/k (see (2.9), (2.12)), where k is from the set $\{2; 2.7; 3; 4\}$. The values of all other parameters are defined in (4.2). The white circles show experimental data, and the solid lines are numerical solutions.

4.2. Simulation of Real Experiment

Microreactor was modelled as a hemi-ellipsoid of revolution in simulation of the behavior of amperometric biosensor based on carbon paste electrode (CPE) encrusted with the microrector. MR was placed on the center of the base of the buffer solution (container). Approximately, 60% of the volume of MR was loaded with the glucose oxidase (GO), and the rest part of MR was the CPC-silica carrier (CPC), i.e., the ratio $c = 0.6$ in (2.7-2.8).

The solution (3.19) - (3.38) with (4.1) of the model was used to simulate the behavior of the biosensor based on the nonhomogeneous MR with the following values of the parameters:

$$
\begin{aligned}
&R = 1\text{cm}, \quad H = 1\text{cm}, \quad R_0 = 0.042\text{cm},\\
&d = 6.7 \times 10^{-6}\text{cm}^2/\text{s}, \quad \overline{d} = d/2.7,\\
&a = 4.4 \times 10^{-5}\text{mol/cm}^3, \quad b = 8.3 \times 10^{-5}\text{mol/cm}^3,\\
&u_0 = 5 \times 10^{-6}\text{mol/cm}^3, \quad n = 2,\\
&\Omega_0 = \{(r,z) : r^2 + (z/0.43)^2 < R_0^2, z > 0\}.
\end{aligned}
\tag{4.2}
$$

The maximal rate of the enzymatic reaction (a) and apparent Michaelis constant (b) was calculated following [31]. The result of calculations as well as experimental data is depicted in figure 4.1. The value $d/2.7$ was chosen as the homogenized diffusion rate $\overline{d}$ in the area of MR to have the best fit between the experimental and numerical curves of the current.

4.3. Influence of the Size of a Microreactor

The dynamics of the biosensor current was considered in a parameterization of the radius of MR, i.e. dependence on the size of a microreactor was considered in the case where the value of the diffusion rate $\overline{d}$ and the values of all other parameters are the same as defined above in (4.2). MR was modelled as a hemisphere. The evolution of a current for the radius of MR equal to $0.25R_0$, $0.5R_0$, R_0, $1.5R_0$, $2.0R_0$ (here R_0 is the same as in (4.2)) is presented in figure 4.2.

One can see that the values of the current (including the maximal current) increase if the radius of a microreactor increases and this growth is non-linear.

4.4. Influence of the Shape of a Microreactor

Several other geometrical shapes of MR differing from the hemisphere were used to analyze a dependence of the operation of biosensor on the form of MR.

Firstly, MR was modelled as a hemiellipsoid of revolution. In the Cartesian coordinate system it is given by

$$
\frac{x^2}{a^2} + \frac{y^2}{a^2} + \frac{z^2}{c^2} < 1, \quad z > 0, \tag{4.3}
$$

where a and c are semi-axes of the ellipsoid. The current was calculated for several different values of a and c keeping the volume of every ellipsoid equal to the volume of a sphere of radius R_0 in order to have the same

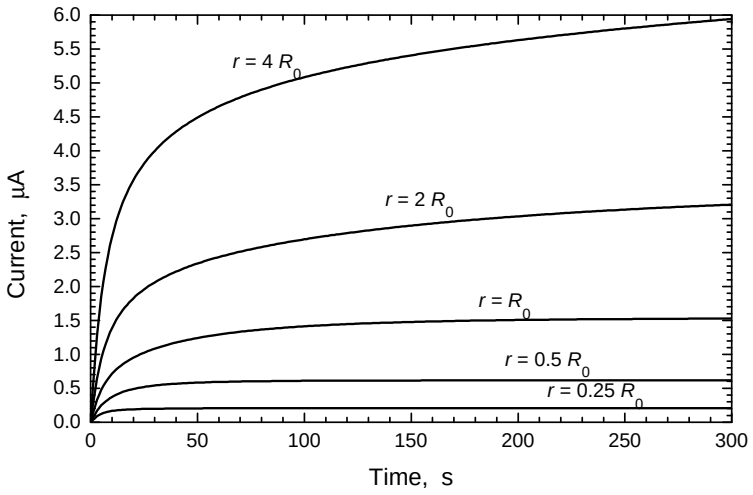

Fig. 4.2: The dependence of the biosensor current on the size of a microreactor solid. The microreactor was modelled as one half of a sphere of radius r, where r is from the set $\{ 0.25R_0; 0.5R_0; R_0; 1.5R_0; 2.0R_0 \}$. R_0 and the values of all other parameters are defined in (4.2).

volume of MR as that used in real experiments and in test calculations. Thus, the volume of MR was kept constant, and only a geometrical form was changed. The following cases were analyzed:

a) the semi-axis c is equal to the one-fourth of the semi-axis a;
b) the semi-axis c is equal to the one-half of the semi-axis a;
c) the semi-axis c is equal to the semi-axis a;
d) the semi-axis c is twice as long as the semi-axis a;
e) the semi-axis c is four times the semi-axis a.

The results of calculation are presented in figure 4.3. The form of MR appears to be important for the current and it is especially important at the initial stage of the reaction. Here the current grows faster as the area of

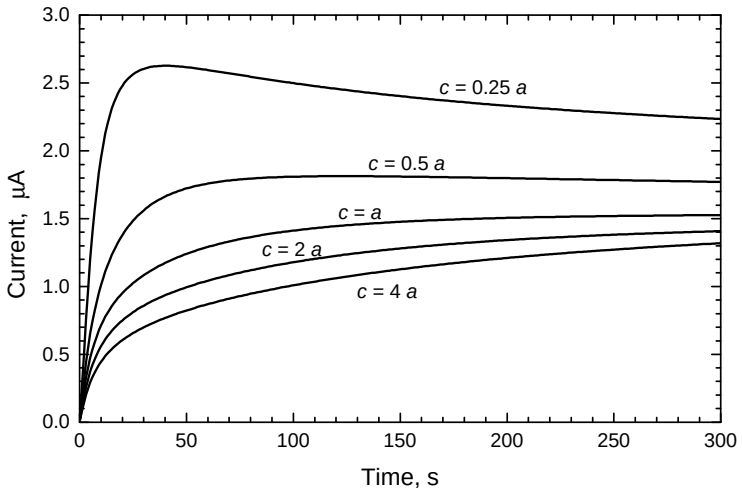

Fig. 4.3: The dynamics of the biosensor current in the case where microreactor is a hemi-ellipsoid of revolution. a and c are, respectively, the semi-axes of the ellipsoid in the $x-$ and $z-$ direction (in the Cartesian coordinate system, see (4.3)). The volume of every ellipsoid is equal to the volume of a sphere of radius R_0.

the base of MR increases. Later this importance decreases. The area of the base of MR is important for the maximal current and the time moment of the occurrence of the maximal current. The maximal value of the current increases and the time moment of its occurrence decreases as the area of the base increases even if the volume of MR remains unchanged.

A half of a torus was used as a second geometrical shape of MR. Let r be the radius of a circle which draws the torus and R is the radius of the leading circle of the torus, i.e., R is the distance between the z-axis and the center of a circle which is rotated around the z-axis. The center of the rotating circle is on the plane $z = 0$. Several different values of both radiuses r and R were used to determine the dependence of the current on

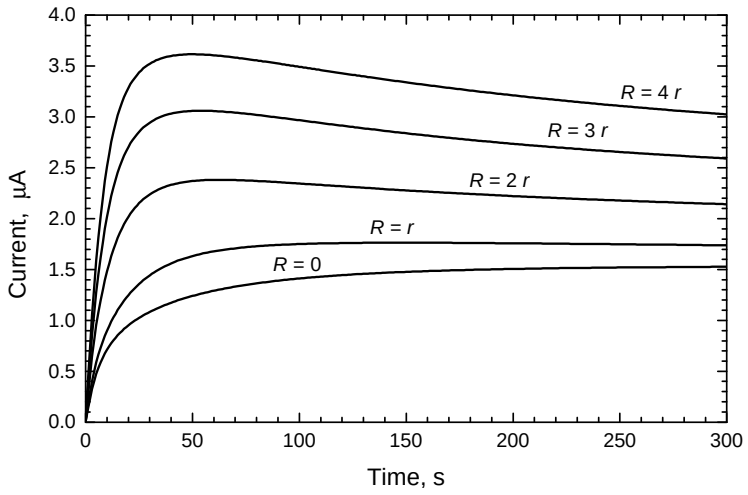

Fig. 4.4: The dynamics of the biosensor current in the case where the microreactor is a half of a torus. r is the radius of the leading circle rotated to get the torus and R is the radius of that rotation around z-axis (in the Cartesian coordinate system). The center of the leading circle is on the plane $z = 0$. The volume of every torus is equal to the volume of a sphere of radius R_0 (4.2).

this geometrical form of MR. The volume of every torus was equal to the volume of a sphere of radius R_0 (see (4.2)). Microreactors of the shape of the upper part of a torus ($z > 0$) were used in calculation. In a special case, where $R = 0$, MR is a half of a sphere. The dynamics of the current in the case where MR was modelled as one half of a torus is depicted in figure 4.4.

4.5. Influence of the Position of a Microreactor

In all the numerical experiments discussed above as well as in the physical experiments, MR was placed on the base of a container. We investigated

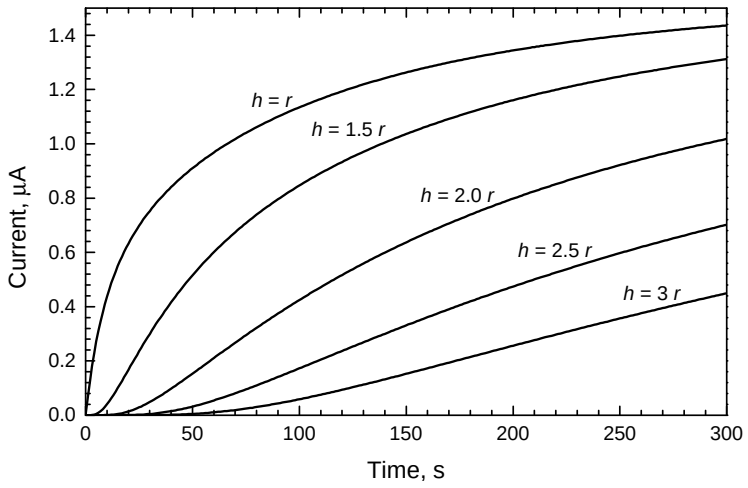

Fig. 4.5: The dynamics of the biosensor current in the case where the microreactor is lifted up from the base of the container. MR is a sphere of radius r. The volume of the sphere is equal to the volume of a hemisphere of radius R_0 (see (4.2)). h is the distance between the center of MR and the base of a container.

the dynamics of the current when MR was lifted up. Since the current arises only when some concentration of the reaction product is reached on the base of the container, the current emerges with delay if MR is lifted up. The time of delay depends on an altitude. The MR in the form of a sphere was used in the analysis. The radius of MR to be lifted up was derived from R_0 (R_0 is defined in (4.2)) to have the volume of MR the same as it was in the test experiments, where MR was modelled as a hemisphere. Let h be the altitude of MR, more precisely, h is the distance between the center of MR and the base of a container. The results of numerical experiments for several values of altitude h are shown in figure 4.5. It appears that the altitude of MR is very important for the dynamics of the biosensor current.

The delay increases and the current grows much slower if altitude increases.

5. Simulation of the electrochemical Behavior of Electrodes

The numerical solution (3.19) - (3.38) of the generalized problem (3.1)-(3.11) was used for digital simulation of electrochemical behavior of partially blocked electrodes under linear potential sweep conditions.

The mathematical model (2.17)-(2.23), (2.26) of the electrochemical behavior of partially blocked electrodes under linear potential sweep conditions was expressed as a special case of the model (3.1) - (3.11) assuming the following:

$$\begin{array}{l} u = C_R, \quad v = C_O, \\ \delta_1 = \delta_R, \quad \delta_2 = \delta_O, \\ A = a, \quad R = b, \quad B = h, \\ G_1 = \Omega_R, \quad G_2 = \Omega_O, \quad G_0 = \emptyset, \\ \Gamma_1 = \Gamma_R, \quad \Gamma_2 = \Gamma_O, \\ \Gamma_{act} = \{(r,z) : 0 \le r \le a, z = 0\}, \\ u_0(r,z) = C_R^0, \quad v_0(r,z) = C_O^0, \\ d_1(r,z) = D_R, \quad d_2(r,z) = D_O, \end{array} \tag{5.1}$$

$$\begin{aligned} \varphi_{11}(r,t) &= nFD_R, \\ \varphi_{12}(r,t) &= -i_0 \left(\frac{1}{C_R^0} \exp\left(-\frac{\alpha nF}{RT} \left(E_{eq} - E(t) \right) \right) \right), \\ \varphi_{13}(r,t) &= i_0 \left(\frac{1}{C_O^0} \exp\left(\frac{(1-\alpha)nF}{RT} \left(E_{eq} - E(t) \right) \right) \right), \end{aligned} \tag{5.2}$$

$$\begin{aligned} \varphi_{21}(r,t) &= nFD_O, \\ \varphi_{22}(r,t) &= -i_0 \left(\frac{1}{C_O^0} \exp\left(\frac{(1-\alpha)nF}{RT} \left(E_{eq} - E(t) \right) \right) \right), \\ \varphi_{23}(r,t) &= i_0 \left(\frac{1}{C_R^0} \exp\left(-\frac{\alpha nF}{RT} \left(E_{eq} - E(t) \right) \right) \right), \end{aligned} \tag{5.3}$$

$$\psi_{11}(r,z) = \begin{cases} 0, & (r,z) \in \Gamma_R^N, \\ 1, & (r,z) \in \Gamma_R \setminus (\Gamma_R^N \cup \Gamma_{act}), \end{cases}$$
$$\psi_{12}(r,z) = \begin{cases} 1, & (r,z) \in \Gamma_R^N, \\ 0, & (r,z) \in \Gamma_R \setminus (\Gamma_R^N \cup \Gamma_{act}), \end{cases} \tag{5.4}$$
$$\psi_{13}(r,z) = \begin{cases} C_R^0, & (r,z) \in \Gamma_R^N, \\ 0, & (r,z) \in \Gamma_R \setminus (\Gamma_R^N \cup \Gamma_{act}), \end{cases}$$

$$\psi_{21}(r,z) = \begin{cases} 0, & (r,z) \in \Gamma_O^N, \\ 1, & (r,z) \in \Gamma_O \setminus (\Gamma_O^N \cup \Gamma_{act}), \end{cases}$$
$$\psi_{22}(r,z) = \begin{cases} 1, & (r,z) \in \Gamma_O^N, \\ 0, & (r,z) \in \Gamma_O \setminus (\Gamma_O^N \cup \Gamma_{act}), \end{cases} \tag{5.5}$$
$$\psi_{23}(r,z) = \begin{cases} C_O^0, & (r,z) \in \Gamma_O^N, \\ 0, & (r,z) \in \Gamma_O \setminus (\Gamma_O^N \cup \Gamma_{act}). \end{cases}$$

The current of the unit cell $I(t)$ (2.24) can be calculated by (3.12). Then, the current of the unit cell was multiplied by the number of the unit cells m to get the total current of the electrode. Since the area S of the whole surface of the model electrodes was approximately 0.48cm^2, and the radius b of unit cell was 23.6μm, then m was about 27430 ($m = S/(\pi b^2)$).

5.1. Experimental

Several model electrodes were used in real experiments and numerical simulation of the behavior of the electrodes. Experimental results were published in [32]. The electrodes varied in the blocking degree $\theta(\theta = 1 - a^2/b^2)$. The geometrical data of model electrodes, used in the real experiments, is presented in table 1. We had no possibility to measure precisely the thickness h of resist layer. The measurement of the resist layer of the model electrodes showed that the thickness was about 1μm ($h \approx 1\mu$m).

Table 1. Geometrical data of model electrodes

No.	a (μm)	b (μm)	θ
1	23.6	23.6	0
2	10.0	23.6	0.82
3	2.5	23.6	0.989

The solution (3.19) - (3.38) with (5.1)-(5.5) of the model (3.1) - (3.11) was used to simulate the electrochemical behavior of the partially blocked

electrodes under linear potential sweep conditions with following values of the parameters:

$$\begin{aligned} &C_R^0 = C_O^0 = 2.5 \times 10^{-5}\text{mol/cm}^3, \\ &D_R = 4.8 \times 10^{-6}\text{cm}^2/\text{s}, \quad D_O = 5.8 \times 10^{-6}\text{cm}^2/\text{s}, \\ &n = 1, \quad \alpha = 0.5, \quad T = 293^o\text{K}, \\ &E_{eq} = 470\text{mV}, \quad E_r = -100\text{mV}, \quad \overline{E} = 900\text{mV}, \end{aligned} \tag{5.6}$$

where E_r is the electrode potential at the reversal time t_r, i.e., $E_r = E(t_r)$ in (2.25), $\overline{E}$ is the final electrode potential. The value of t_r for the numerical simulation of the electrode behavior, was calculated from (2.25) with the value E_r and a value of the sweep rate v. The electrode potential during the experiments, was decreased (forward or cathodic sweep direction) from E_{eq} to E_r, then the electrode potential was increased (reverse or anodic sweep direction) up to $\overline{E}$. There were two sweep rates (v): 20mV/s and 100mV/s. In all the numerical experiments, values of i_0 in (2.23), (5.3), (5.3) and δ_R, δ_O in (2.26), (5.1) were chosen to have the best fit between the experimental data and numerical solutions as values of the current. In addition, the values of i_0 were chosen among values between 0.01 and 0.1 (A/cm^2) [20]. An empirical law of $\delta_R\sqrt{v} \approx const$ and $\delta_O\sqrt{v} \approx const$, which was found to be valid under linear potential sweep condition [33], was used to determine values of δ_R, δ_O.

The values (5.6) of the parameters were constant in numerical simulation of the all experiments.

5.2. Simulation of the Behavior of the unblocked Electrode

Firstly, the model was used for numerical simulation of the unblocked electrode (No. 1 in table 1). There are no inactive sites at all in this extreme case of the blocking degree. So, $a = b$, $h = 0$ with $\theta = 0$. The thickness δ_O and δ_R of the Nerst diffusion layer was chosen as $\delta_O = 240\mu$m, $\delta_R = 420\mu$m at $v = 20$ mV/s and $\delta_O = 110\mu$m, $\delta_R = 190\mu$m at $v = 100$ mV/s.

In numerical solution, accurate and stable results were achieved when the radius a of the active site of the unit cell was divided into 50 increments, and the minimum step in z direction was equal to $\min(\delta_O, \delta_R)/10^3$ (0.24μm at $v = 20$ mV/s and 0.11μm at $v = 100$ mV/s). The step in t direction was 10^{-2} s at $v = 20$ mV/s and 2×10^{-3} s at $v = 100$ mV/s. Results of the calculation are depicted in figure 5.1. As it is possible to notice, the good

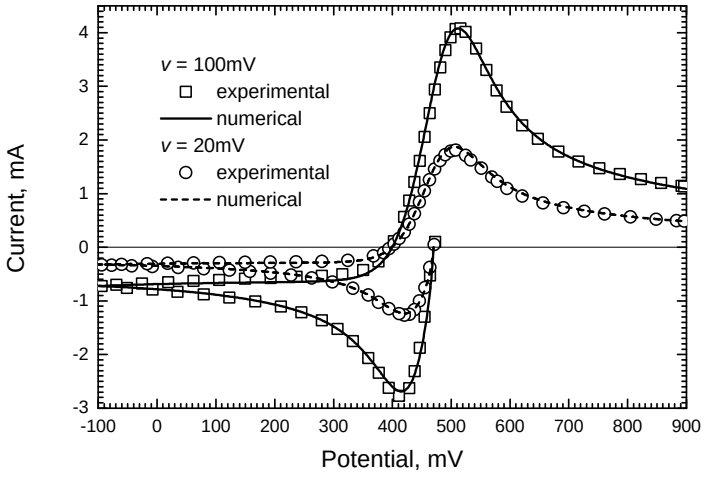

Fig. 5.1: The dynamics of the current for the unblocked electrode No.1 (table 1) at two sweep rates v: 100 mV/s (i_0 = 0.015A/cm^2, δ_O = 110μm, δ_R = 190μm) and 20 mV/s (i_0 = 0.012A/cm^2, δ_O = 240μm, δ_R = 420μm). The white squares and circles show experimental data, and the solid and dash lines are corresponding numerical solutions at v = 100 mV/s and v = 20 mV/s, respectively.

agreement between the result of the calculation and experimental data is obtained.

5.3. Simulation of the Behavior of the partially blocked Electrodes

Then the electrochemical behavior of several partially blocked electrodes (No. 2 and 3 in table 1) was simulated. At first, we did not take into account the resist layer, following the known assumption [20] that the influence of the thickness of the resist layer of $1 - 2\mu$m would be negligible because of the thickness is much smaller than the radius of the unit cell. Results of calculations showed that calculated maximal currents were rather

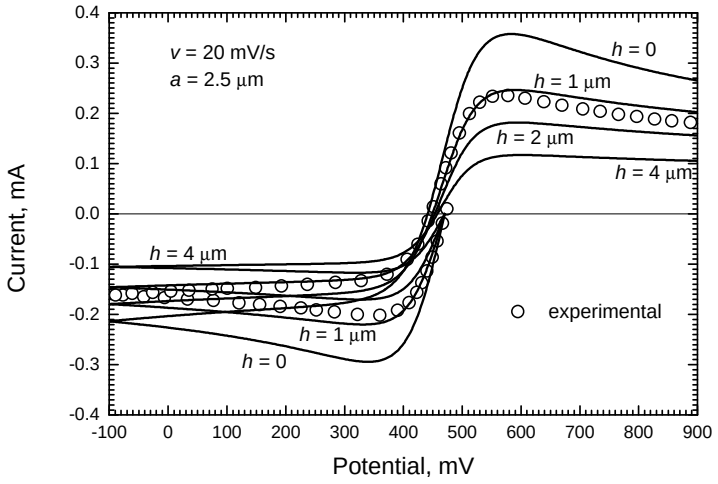

Fig. 5.2: The dynamics of the current for model electrode No.3 (table 1) at sweep rate $v = 20$ mV/s. h is the thickness of resist layer, where h is from set $\{0, 1, 2, 4\}$ (μm), $\delta_O = 280\mu$m, $\delta_R = 340\mu$m and $i_0 = 0.1\text{A/cm}^2$. The white circles show experimental data, and the solid lines are numerical ones.

greater (up to 40% than the experimental maximal currents. Therefore, the resist layer was introduced into the mathematical model (2.17)-(2.23), i.e., into the definition of the diffusion space Ω_O and Ω_R (2.26) of the model (2.17)-(2.23).

The thickness δ_O and δ_R of the Nerst diffusion layer in modelling of electrodes No. 2 and 3 (see table 1), was chosen as $\delta_O = 280\mu$m, $\delta_R = 340\mu$m at potential sweep rate v of 20 mV/s and $\delta_O = 125\mu$m, $\delta_R = 150\mu$m at $v = 100$ mV/s. Accurate and stable results of numerical simulation were achieved when the radius a of the active site of the unit cell was divided into 200 increments, i.e., the minimum step was 0.05μm for electrode No.2 and 0.0125μm for electrode No.3, while the minimum step was 0.47μm in

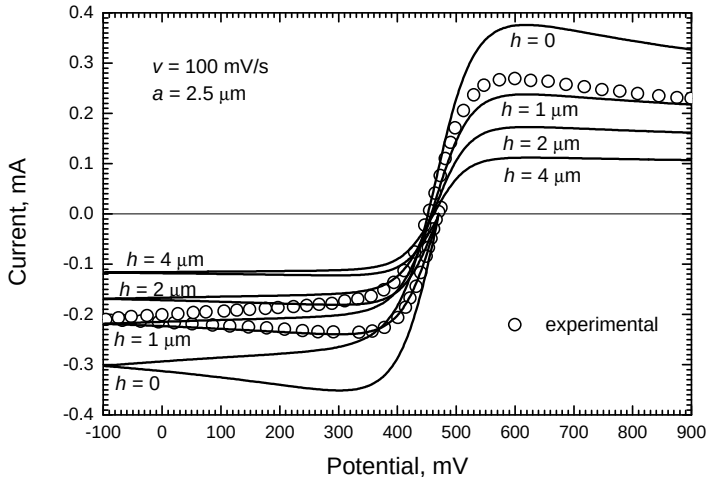

Fig. 5.3: The dynamics of the current for model electrode No. 3 (table 1) at sweep rate $v = 100$ mV/s. The thickness h of the resist layer is from set $\{0, 1, 2, 4\}$ (μm). $\delta_O = 125\mu$m, $\delta_R = 150\mu$m and $i_0 = 0.1\text{A/cm}^2$. The white circles show experimental data, and he solid lines are numerical ones.

the case of the unblocked electrode No.1. The minimum step in z direction was used as $\min(\delta_O, \delta_R)/10^4$ (0.028μm at $v = 20$ mV/s and 0.0125μm at $v = 100$ mV/s). So, the minimum step of the discrete grid $\widehat{\omega}_1$ and $\widehat{\omega}_2$ in both space directions (r, z) was of the order of magnitude lower than the corresponding minimum step in numerical modelling of the unblocked model electrode. It can be explained by the discontinuity of the boundary condition (2.21)-(2.22) and relatively small thickness h of the resist layer (h was from set $\{1, 2, 4\}(\mu\text{m})$), i.e., $h \ll \min(\delta_O, \delta_R)$). The step in t direction was the same as in modelling of the unblocked electrode. In numerical modelling of an extreme case of $h = 0$, the minimum step in z direction was the same as in case of unblocked electrode. Results of the calculations

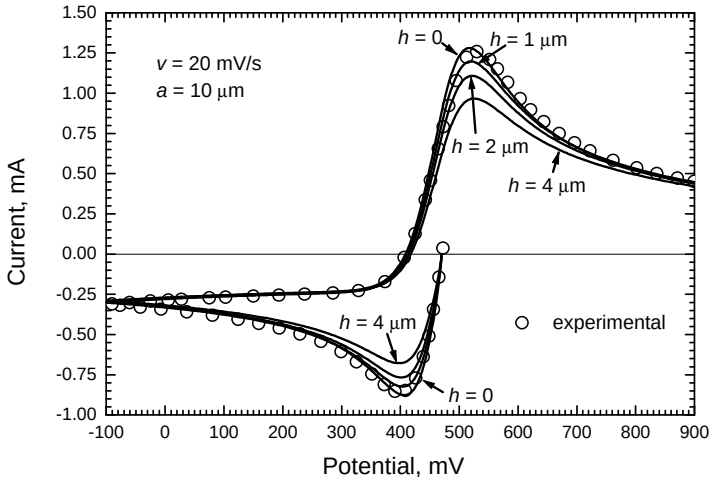

Fig. 5.4: The dynamics of the current for model electrode No. 2 (table 1) at sweep rate $v = 20$ mV/s. Values of δ_O, δ_R, and i_0 are the same as in figure 5.2. The thickness h of the resist layer is from set $\{0, 1, 2, 4\}$ (μm). The white circles show experimental data, and the solid lines are numerical ones.

are depicted in figures 5.2, 5.3, 5.4.

5.4. The Influence of the Thickness of the resist Layer

The influence of the thickness of the resist layer as seen in figures 5.2 and 5.3, appears to be important for highly blocked electrode ($\theta = 0.989$). The good agreement between the calculated and experimental results is obtained at resist layer thickness (h) of about 1μm. That value of the thickness compare favorable with the values given by experimental measurement of the resist layer of the model electrodes. Figures 5.2 and 5.3 show that the cathodic (forward) and anodic (reverse) maximal currents are about $25 - 40\%$ less for the thickness h of the resist layer of 1μm in comparison with the case

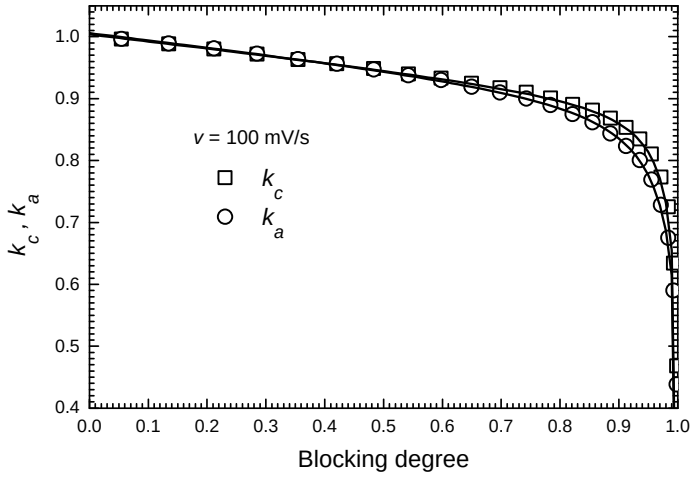

Fig. 5.5: The dependence of the normalized cathodic (k_c) and anodic (k_a) (see (5.7)) peak current on the blocking degree θ at sweep rate $v = 100$ mV/s. Values of δ_O and δ_R are the same as in figure 5.3, $i_0 = 0.05\text{A/cm}^2$. The white rectangles and circles show calculated values of k_c and k_a, respectively. The solid lines are corresponding functions (5.8) fitted to these values.

of $h = 0$. This property is valid for both sweep rates: 20 mV/s (figure 5.2) and 100 mV/s (figure 5.3).

While comparing figure 5.2 with figure 5.4, one can see that the influence of the resist layer on values of the current is less meaningful for an electrode with the less blocking degree at the same sweep rate. In other words, the effect of the resist layer is more enhanced with the increase of the blocking degree.

The investigation of the influence of the resist layer on the behavior of the partially blocked electrodes was generalized. Let $I^c_{h,\theta}$ be the cathodic peak current and $I^a_{h,\theta}$ the anodic one for the model electrode with blocking

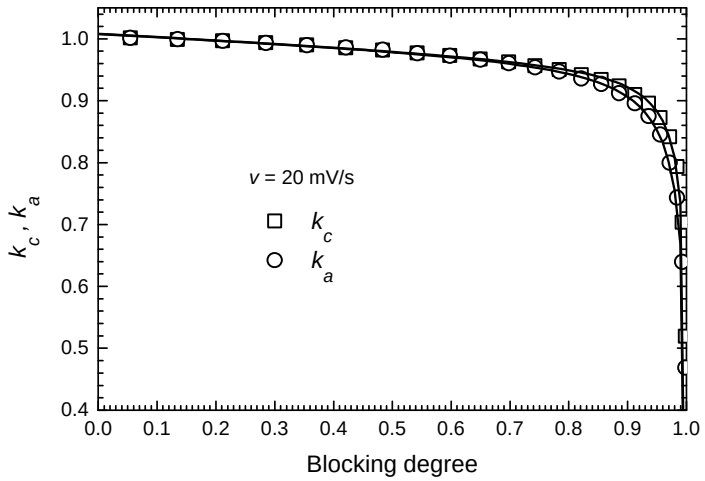

Fig. 5.6: The dependence of the normalized cathodic (k_c) and anodic (k_a) (see (5.7)) peak current on the blocking degree θ at sweep rate $v = 20$ mV/s. Values of δ_O and δ_R are the same as in figure 5.2, $i_0 = 0.05\text{A/cm}^2$. The white rectangles and circles show calculated values of k_c and k_a, respectively. The solid lines are corresponding functions (5.8) fitted to these values.

degree of θ and the resist layer thickness of h (μm). Values of $I^c_{h,\theta}$ and $I^a_{h,\theta}$ were calculated for various values of the parameter $\theta (0 < \theta < 1)$ and two values of h: 0 (no resist layer) and 1μm. Let k_c be a dimensionless ratio of the cathodic peak current $I^c_{1,\theta}$ to $I^c_{0,\theta}$, and k_a a ratio of the anodic peak current $I^a_{1,\theta}$ to $I^a_{0,\theta}$, i.e.,

$$k_c = I^c_{1,\theta}/I^c_{0,\theta}, \quad k_a = I^a_{1,\theta}/I^a_{0,\theta}. \tag{5.7}$$

Figure 5.5 shows the variation of the ratio k_c and k_a with blocking degree. In this calculation, values of $v = 100$ mV/s, $\delta_O = 125\mu$m, $\delta_R = 150\mu$m, and $i_0 = 0.05\text{A/cm}^2$ were employed.

Curves drawn through all calculated values are functions:

$$(1-\theta)(p_1/(p_2-\theta)+p_3/(p_4-\theta)+p_5), \tag{5.8}$$

where $p_1 = 0.611$, $p_2 = 1.001$, $p_3 = 0.293$, $p_4 = 1.02$, $p_5 = 0.106$ for k_c and $p_1 = 0.597$, $p_2 = 1.001$, $p_3 = 0.316$, $p_4 = 1.04$, $p_5 = 0.104$ for k_a.

A significant decrease in k_c as well as k_a with the increase in the blocking degree can be seen in figure 5.5. Note the $k_c \approx k_a \approx 1$, i.e., $I^c_{1,\theta} \approx I^c_{0,\theta}$ and $I^a_{1,\theta} \approx I^a_{0,\theta}$ when blocking degree θ becomes about 0 . Values of k_c and k_a notable decrease for higher values of the blocking degree $\theta(\theta >\approx 0.85)$. So, the resist layer of thickness of 1μm appears to be important for the peak currents, and it is especially important for highly blocked electrodes. Particularly, the sensitivity of the cathodic peak current and anodic one to the thickness of the resist layer is very similar.

The similar variation of the ratio k_c and k_a with blocking degree was also determined at the sweep rate $v = 20$ mV/s . This is depicted in figure 5.6. In this calculation, values of $\delta_O = 280\mu$m, $\delta_R = 340\mu$m, and $i_0 = 0.05\text{A/cm}^2$ were employed. Curves drawn through all calculated values are functions (5.8), where $p_1 = 0.715$, $p_2 = 1.001$, $p_3 = 0.251$, $p_4 = 1.02$, $p_5 = 0.048$ for k_c and $p_1 = 0.608$, $p_2 = 1.001$, $p_3 = 0.366$, $p_4 = 1.02$, $p_5 = 0.042$ for k_a.

6. Conclusions

The homogenization process [10] can be successfully used to reduce the mathematical model of the operation of a biosensor based on the non-homogeneous microreactor. The homogenized problem can be effectively solved by using finite-different technique.

The mathematical model (2.17)-(2.23) may be successfully used for the simulation of electrochemical behavior of partially blocked as well as unblocked electrodes. The mass transport may be assumed to be regular in the entire diffusion space. In simulation of behavior of the partially blocked electrodes, the resist layer of thickness of 1μm should be taken into account to obtain the good agreement between experimental and numerical results for highly blocked electrodes ($\theta >\approx 0.85$). The thickness of the resist layer is a parameter of the model, which can be measured experimentally, in contrast to the parameter γ in [20], which had a physical sense but was, in fact, a fitting parameter. The influence of the resist layer on the cathodic and anodic peak current increases with the blocking degree.

References

1. Clark C. M., *How should we respond to the worldwide diabetes epidemic?*, *Diabetes Care*, **21(4)**, p. 475-476, 1998.

2. Zimmet P., McCarty D., *The NIDDM epidemic: global estimates and projection: a look into the crystal ball*, *IDF Bulletin*, **40(3)**, p. 8-16 , 1995.

3. Turner A.P.F., Karube I., Wilson G.S. *Biosensors: Fundamentals and Applications*, *Oxford University Press, Oxford*, p. 770, 1987.

4. Kulys J., Palaima A. and Urbelis G., *Employing heterocyclic dihydropolyazines for amperometric glucose sensing, Anal. Lett.*, **31(4)**, p. 569-584, 1998.

5. Kulys J., *Carbon paste electrode encrusted with a microreactor as a glucose biosensor, Biosens. Bioelectr.*, **14**, p. 473-479, 1999.

6. Clark L. C., Lyons C. *Electrode system for continuous monitoring in cardiovascular surgery*, *Ann. N.Y. Acad. Sci.*, **102**, p.29-45, 1962.

7. Sorochinskii V.V., Kurganov B.I., *Steady-state kinetics of cyclic conversions of substrate in amperometric bienzyme sensors*, *Biosens. Bioelctr.*, **11**, p. 225-238, 1996.

8. Lide D. R., ed., *Handbook of Chemistry and Physics*, *74th Edition*, CRC Press, Boca Raton, Ann Arbor, London, Tokyo, 1993-1994.

9. Wightamm R.M. and Wipf D.O., *In: Electroanalytical Chemistry, ed. A.J. Bard*, *M. Dekker*, New York, Vol. 15, p. 267-353, 1989.

10. Bakhvalov N. S. and Panasenko G. P., *Homogenisation of Processes in Periodic Medium*, [in Russian], *Nauka, Moskow*, 1984.

11. Aoki K., *Electroanalysis*, **5**, p. 627, 1993.

12. Scharifker B.R., *J. Electroanalyt. Chem.*, **240**, p. 61, 1988.

13. Lee C., Miller C.J. and Bard A.J., *Analyt. Chem.*, **63**, p. 78, 1991.

14. Reller H., Kirowa-Eisner E. and Gileadi E., *J. Electroanalyt. Chem.*, **138**, p. 65, 1982.

15. Reller H., Kirowa-Eisner E. and Gileadi E., *J. Electroanalyt. Chem.*, **161**, p. 247, 1984.

16. Tokuda K., Gueshi T. and Matsuda H., *J. Electroanalyt. Chem.*, **102**, p. 41, 1979.

17. de Oliveira P., Jiang L., Kaneko S. , Aitken A., Leigh P. A., Dobson P.J. and Hill H. A. O., *45 th Annual ISE Meeting*, Porto, P. OVI-4, 1994 .

18. Horrocs B.R., Mirkin M.V., Pierce D.T., Bard A.J., Nagy G. and Toth K., *Analyt. Chem.*, **65**, p. 1213, 1993.

19. Aoki K., Morita M., Niwa O. and Tabei H., *J. Electroanalyt. Chem.*, **256**, p. 269, 1988.

20. Gueshi T., Tokuda K. and Matsuda H., *Voltammetry at partially covered electrodes. Part I. Chronopotentiometry and chronoamperometry at model electrodes*, *J. Electroanal. Chem.*, **89**, p. 247, 1978.

21. Gueshi T., Tokuda K. and Matsuda H., *Voltammetry at partially covered electrodes. Part II. Linear potential sweep and cyclic voltammetry*, *J. Electroanal. Chem.*, **101**, p. 29-38, 1979.

22. Deslous C., Gabrielli C., Keddam M., Khalil A., Rosset R., Trobollet B. and Zidoune M., *Impedance techniques at partially blocked electrodes by scale deposition Electrochim. Acta*, **42**, p. 1219-1233, 1997.

23. Hitzig J., Titz J., Juttner K., Lorenz W.J. and Schmidt E., *Electrochim. Acta*, **29**, p. 287, 1984.

24. Schmidt E., Hitzig J., Titz J., Juttner K. and Lorenz W.J., *Inhomogeneous electrodes - a polarization model of the partially blocked reversible metal ion electrode*, *Electrochim. Acta*, **31**, p. 1041-1050, 1986.

25. Bard A.J., *Analyt. Chem.*, **33**, p. 11, 1961.

26. Baronas R., Ivanauskas F. and Kulys J., *Modelling a biosensor based on the heterogeneous microreactor*, *J. Math. Chem.*, **25**, p. 245-252, 1999.

27. Yokoyama K., Kayanuma Y., *Cyclic Voltammetric Simulation for Electrochemically Meddiated Enzyme Reaction and Determination of Enzyme Kinetic Constants*, *Anal. Chem.*, **70**, p. 3368-3376 , 1979.

28. Samarskii A.A., *The theory of difference schemes*, [in Russian], *Nauka*, Moskow, 1989.

29. Buda V., Sapagovas M. and Čiegis R., *A two-dimensional model of non-linear diffusion*, *Mathematical and mechanical modelling in microelectronics*, [in Russian], Institute of Physics of Semiconductors, Vilnius, p. 36-43, 1985.

30. Buda V., Čiegis R. and Sapagovas M., *A model of multiple diffusion from the restrict origin*, *Differential equations and their application* [in Russian], Institute of Mathematics and Cybernetics, Vilnius, **38**, p. 9-14, 1986.

31. Weibel K., Bright H. J., *The glucose oxidase mechanism*, *J. Biol. Chem.*, **246**, p. 2734-2744, 1971.

32. Survila A., Stasiukaitis P.V., Kanapeckaitė S. and Uksienė V., *Chemija*, **2**, Vilnius, p. 143, 1998.

33. Survila A., Stasiukaitis P.V. and Kanapeckaitė S., *Chemija*, **2**, Vilnius, p. 138, 1998.

34. Babloyantz A., Salazar J. M., Nicolis C., *Evidence of chaotic dynamics of brain activity during the sleep cycle, Phys. Lett. A*, **111A**, p. 152, 1985.